Remaining energy estimation for lithium-ion batteries via Gaussian mixture and Markov models for future load prediction

Mona Faraji Niri [a*], Truong MN Bui [a], Truong Q Dinh [a], Elham Hosseinzadeh [a], Tung Fai Yu [b], James Marco [a]

[a] Warwick Manufacturing Group, University of Warwick, Coventry, CV4 7AL, United Kingdom, (Emails: Mona.Faraji-Niri@warwick.ac.uk, t.bui.2@warwick.ac.uk, T.Dinh@warwick.ac.uk, E.Hosseinzadeh@warwick.ac.uk, James.Marco@warwick.ac.uk,)

[b] Advanced Battery Engineering, Jaguar Land Rover Ltd, Coventry, CV3 4LF, United Kingdom, (Email: tyu5@jaguarlandrover.com)

Abstract:

Other than upgrading the energy storage technology employed within electric vehicles (EVs), improving the driving range estimation methods will help to reduce the phenomena, known as range anxiety. The remaining discharge energy (RDE) of the battery affects the remaining driving range of the vehicle directly and its accurate calculation is crucial. In this paper a novel approach for the RDE calculation of the battery is proposed. First a stochastic load prediction algorithm is prepared via a Markov model and Gaussian mixture data clustering. Then, the load prediction algorithm is connected to the battery second order equivalent circuit model (ECM) coupled with a bulk parameter thermal model. Based on the extrapolated load and the battery dynamics, the battery future temperature conditions, future parameter variations and its internal states are predicted. Finally, the battery end of discharge time is prognosed and its RDE is calculated iteratively. In order to prove the proposed concept, lithium-ion battery cells are selected and the performance of the method is validated experimentally under real-world dynamic current charge/discharge profiles.

Keywords: Gaussian mixture data clustering; Markov model; transient load; lithium-ion battery; remaining energy prediction; end of discharge time prognosis

1. Introduction

Electric vehicles are one of the main candidates for reducing the dependency of the future transportation systems on traditional combustion fuels. Although the technology that underpins their deployment has advanced in recent years, their full integration into the transportation systems is still largely limited due to the higher cost, limited charging infrastructure and relatively short driving range compared to traditional vehicles. The limited driving range of an EV is reported to be one of the most significant factors that affects its acceptance and causes range anxiety [1]. Obviously improving battery energy capacity, efficiency of the other powertrain components, as well as the correct estimation of the remaining driving range can help to reduce the range anxiety [2, 3]. The RDE of the battery together with the average vehicle energy consumption, reveals its remaining driving range, therefore an accurate estimation of RDE of the vehicle is necessary. Traditionally, SoC is considered as an indicator of the remaining energy of the battery [4]. However SoC indicates the capacity not actual energy [5] and compared to the large number of publications on SoC estimation challenges [4, 6, 7], fewer material are published for the remaining energy estimation.

The RDE of a battery is given by (1) where I is the battery input current, U_T is the terminal voltage and $EoDT_t$ is the end of discharge time (EoDT).

$$RDE_t = \int_t^{EoDT_t} U_{Tt} I_t dt \tag{1}$$

Three main definitions can address the EoDT, (*i*) the time when the SoC reaches a predetermined lower limit [8], (*ii*) the time when the terminal voltage reaches a lower threshold cut-off voltage [9], (*iii*) the time

when the battery temperature hits a lower or upper limit. While the temperature and voltage cut-off limits are normally set via battery cell manufacturer's recommendation, the SoC limit may be selected dependent to the use case and the preferred safety and reserved margins [8, 10, 11, 12]. Based on either definitions of EoDT, remaining discharge time (RDT) is the defined as $RDT_t = EoDT_t - t$.

One convenient way to calculate the RDE is direct calculation (DC) via (2) Where *OCV* is the battery open circuit voltage and *Q* is its standard capacity.

$$RDE_t = Q.U_{OC}(SoC_t).(SoC_t - SoC_{EoDT}) \quad (2)$$

DC assumes that the terminal voltage is equal to $U_{OC}(SoC_t)$ and remains unchanged during the whole RDE calculation range, which is a very conservative assumption. This method, although simple, cannot provide accurate results especially for EV applications with transient load profiles [13]. That is why model-based calculation is addressed in recent studies where an iterative estimation of the battery terminal voltage and SoC is performed [13, 14, 15, 16]. A comprehensive study via ECM is conducted in [13], which reported that the DC method is not accurate, and that keeping the battery parameter unchanged with respect to future discharge conditions causes an error in the RDE value. Conventional model-based RDE or EoDT prediction methods are all sensitive to noises, initial conditions as well as the model uncertainties. To address this challenge, adaptive RDE estimation methods via Kalman filters (KFs) and particle filters (PFs) are proposed [8, 11, 14, 15, 16, 17, 18, 19]. Although these filters mostly focus on the state of energy (SoE) estimation rather than the RDE itself, but they are still significantly useful for vehicle and range estimation applications. In this respect, improved SoE filters by output-feedback correction loops (OFCLs) are designed in [15], [20], [21]. The OFCLs modify the process and measurement noise variance if the prediction error over a horizon gets bigger or smaller than a predefined threshold. A comparison between different KFs and PFs for the EoDT prognosis is given in [12]. Extended adaptive energy estimation schemes based on neural networks [22, 23, 24], and probabilistic models [25] are also stablished to address the concerns regarding uncertainties.

The RDE calculation needs both historical measurements and future forecasts of the battery states as it is a calculation between *t* to EoDT (see equation (1)). In most of the aforementioned studies it is assumed that the future conditions of the battery is *a priori* known. This assumption is limiting as characterization of the battery future load is critically challenging. For example in EVs load depends on driver's behaviour, traffic, road, vehicle and environmental conditions [26]. Definitely, RDE calculation can benefit from predicted information about the battery load and its constraints. Different approaches for battery load prediction are reported in the literature, which use navigation systems, historical data and statistical analysis of the vehicle's energy consumption and driver style on specific roads [27, 28, 29]. However, few of these methods are directly connected to the battery to investigate how they may affect the RDE prediction accuracy. Prediction of the future battery conditions is performed by the mean of the historical data in [16, 30]. By this approach the future load current is equal to the moving average (mean) of the data. This mean-based prediction although conceptually simple, cannot effectively extrapolate the loads with high transitions. In [31] a multi resolution analysis technique based on discrete wavelet transform (DWT) is provided. By DWT the battery historical load is decomposed to high and low frequency data after passing through multiple layers of filters and then used for load reconstruction. The historical-data-based methods are passive prediction algorithms mostly reactive to what has happened without inclusion of any uncertainties or scenarios that might happen in future. To consider the uncertainty of the future conditions, probabilistic and stochastic algorithms are proposed. In [11] the battery future load is characterised through a Gaussian process and in [8], it is addressed through a Markov model with the states of the minimum and maximum of the load in a fixed length window of the historical data. Both methods address the uncertainties in the predicted results but the first approach is still unable to address the transient behaviour of load, and the second approach is still either over estimating or under estimating loads because of its based on the maximum and minimum load value for Markov model states.

Considering the above-mentioned challenges, this paper aims to extend research published in [12, 16, 27, 28, 29, 30]. EoDT/ RDT and RDE prediction of batteries are all long term prediction problems with horizon as long as several hours. The battery parameters as well as its states and temperature may change significantly during the long horizon and cannot be neglected or assumed unchanged.

The novelty of this paper is designing a mechanism to address the battery load characteristics, transitions and its uncertainties for EoDT/ RDT and RDE prediction. Compared to [11, 8, 14, 15, 16, 17, 18] it prepares an online load prediction algorithm and removes the assumption of a priori known loads. As an extension to [13] it predicts the future temperature and schedules the future battery parameters with respect to temperature beside SoC. And finally compared to [16, 30] it boosts the moving average prediction method to make it more appropriate for predictions under transient loads.

This proposed load prediction mechanism is constructed via a Gaussian mixture model to extract the load features as well as Markov model to represent the load transitions. The forecasted load provides an input to a battery ECM coupled with a thermal model to forecast future battery parameters and states. Finally the battery states are utilised to perform the EoDT prognosis and the RDE prediction.

Fig. 1 shows the boundaries of the proposed mechanism, the output of which is transferable to the remaining range estimation mechanism or the battery management system (BMS) itself. To validate the performance of this method, real-world and synthetic drive cycles are converted to a battery input via previously validated EV power train model [32] and used for charge/discharge cylindrical lithium-ion battery cells in different temperatures.

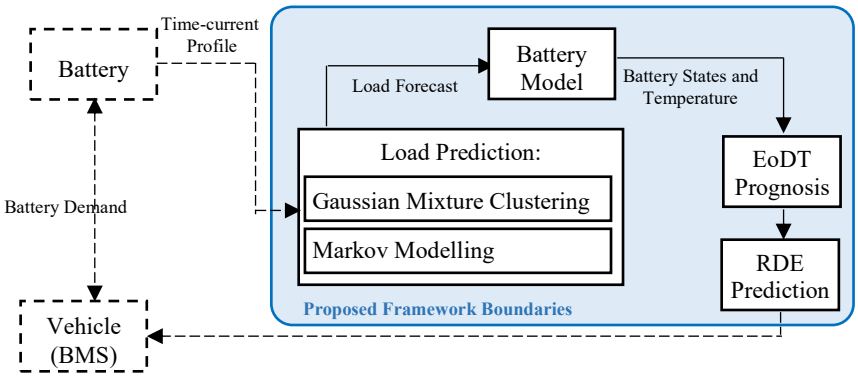

Fig. 1. The boundaries of the designed RDE prediction framework

The remainder of this paper is organized as follows: in Section 2 load characterization and prediction algorithm are proposed. Section 3 defines the battery electrical and thermal model and the EoDT, RDT and RDE prediction. Section 4 includes the experimental results and verification. Finally Section 5 provides conclusions and the Section 6 gives suggestions for further works.

2. Proposed Load Prediction Algorithm

In order to predict the future load, two consecutive steps need to be undertaken as shown on Fig. 1. First to extract the features and information from the historical load data and second to use those features to extrapolate the load and forecast it until the constraints of the battery EoDT are met. To address the behaviour of the load, a combination of the load mean (or expected value), load variance or (standard deviation) and a quantitative measure of transition is suggested here. In this concept, the multiple mean and variance values in a window of the historical data (historical window) are recognized and then used to quantify the transition in the load via the "jumps" between those mean and variance values. The former computational stage is taken via clustering the load data and the latter is addressed via a stochastic modelling approach.

2. 1. Feature extraction by Gaussian mixture data clustering

Data clustering is a type of learning process which determines and distinguishes the attributes of different groups in a data set. It is the process of dividing a data set into a number of classes based on the predefined subset of similarities between them. Gaussian mixture model (GMM) is one powerful framework for representing a dataset and estimate its probability density function (PDF). Examples of its use include image processing [33], emotion recognition [34] and load forecasting [35]. GMM is a mixture of components and when used for clustering a dataset $x:\{x_1, x_2, \ \dots \ , x_T\}$ provides *M* clusters $\{C_1, C_2, \ \dots C_m, C_M\}$ following

Gaussian distribution function of $N(x;\mu_m,\sigma_m)$, with mean μ_m and covariance σ_m. The PDF of dataset, $p(x)$, follows

$$
\begin{aligned}
p(x) &= \sum_{m=1}^{M} w_m p(x \mid m) = \sum_{m=1}^{M} w_m N(x;\mu_m,\Sigma_m) \\
N(x;\mu_m,\Sigma_m) &= \frac{1}{(2\pi)^{1/2}\left|\Sigma_m\right|^{1/2}} \exp\left(-\frac{(x-\mu_m)^T \Sigma_m^{-1}(x-\mu_m)}{2}\right)
\end{aligned}
\tag{3}
$$

where $p(x \mid m)$ is the PDF of cluster C_m and w_m is its associated weight where $\sum_m w_m = 1$. Given a dataset, GMM clustering facilitates a soft clustering [36] in which, data can belong to more than one cluster with different probabilities.

The parameters of a GMM are estimated from the source dataset via maximum likelihood learning [37]. First, the posterior probability, $P(m \mid x)$ of each data point belonging to cluster C_m is calculated by:

$$
P(m \mid x) = \frac{w_m p(x \mid m)}{p(x)} = \frac{w_m p(x \mid m)}{\sum_{m=1}^{M} w_m p(x \mid m)}
\tag{4}
$$

Which follows the total law of probability by $\sum_{m=1}^{M} w_m P(m \mid x) = 1$. Via $P(m \mid x)$ a soft count is estimated as $N_m^* = \sum_{t=1}^{T} P(m \mid x_t)$ and each data point is assumed to be assigned to class C_m based on $P(m \mid x_t)$. So the estimated mean, $\hat{\mu}_m$, variance, $\hat{\sigma}_m$, and weights, $\hat{w}_m$, can be found as (5).

$$
\begin{aligned}
\hat{\mu}_m &= \frac{\sum_{t=1}^{T} P(m \mid x_t) x_t}{\sum_{t=1}^{T} P(m \mid x_t)} = \frac{\sum_{t=1}^{T} P(m \mid x_t) x_t}{N_m^*} \\
\hat{\sigma}_m &= \frac{\sum_{t=1}^{T} P(m \mid x_t) \left\| x_t - \hat{\mu}_m \right\|^2}{\sum_{t=1}^{T} P(m \mid x_t)} = \frac{\sum_{t=1}^{T} P(m \mid x_t) \left\| x_t - \hat{\mu}_m \right\|^2}{N_m^*} \\
\hat{w}_m &= \frac{1}{T} \sum_{t=1}^{T} P(m \mid x_t) = \frac{N_m^*}{T}
\end{aligned}
\tag{5}
$$

Since $p(x \mid m)$ and w_m are required to be known *a priori* to estimate the parameters of $P(m \mid x)$ in (5) and its parameters cannot be obtained in a closed form, an iterative algorithm is necessary. This algorithm is consisted of two parts and called expectation maximization (EM). EM aims to find the set of parameters $\theta_m = (\mu_m, \sigma_m, w_m)$ that maximize the likelihood $L(\theta, x)$ (its logarithm $\log L(\theta, x)$ in convex form) where θ is the whole set of parameters in all clusters [37].

$$
\begin{aligned}
L(\theta, x) &= \prod_{t=1}^{T} p(x_t) = \prod_{t=1}^{T} \sum_{m=1}^{M} w_m p(x_t \mid m) \\
\log L(\theta, x) &= \sum_{t=1}^{T} \log\left(p(x_t)\right) = \sum_{t=1}^{T} \log\left(\sum_{m=1}^{M} w_m p(x_t \mid m)\right)
\end{aligned}
\tag{6}
$$

The first part of EM is computing the probabilities of $P(m|x)$ using the available estimates of $\theta_m = (\mu_m, \sigma_m, w_m)$ and the second part is computing the parameters $\theta_m = (\hat{\mu}_m, \hat{\sigma}_m, \hat{w}_m)$ of each cluster C_m using the available estimate of $P(m|x)$.

2. 2. Feature extraction via Markov modelling

A Markov model in its simplest form is defined via a finite number of states $S = \{S_t, t \geq 0\}$ taking values in the set $\underline{\mathrm{N}} = \{1, 2, \ldots, N\}$. Markov model is a stochastic framework widely used for analysis and prediction of abruptly changing time series and datasets. A dataset is said to follow the Markov property, if the conditional probability of the present state only depends on the probability of one step previous state rather than the probability of the states during the whole history [38]. If the states of the Markov chain are observable, then the change (or jumps) between the states is represented with conditional probabilities of:

$$\Pr\{S_t = j \mid S_{t-1} = i\} = \lambda_{ij} \;\; i, j \in \underline{\mathrm{N}} \tag{7}$$

where $\lambda_{ij} \geq 0$ denotes the transition probability (TP). The TPs follow the total probability rule $\sum_{j=1}^{N} \lambda_{ij} = 1$ and form a unique transition probability matrix (TPM) of (8).

$$\mathbf{\Lambda} = \left[\lambda_{ij}\right], \; i, j \in \underline{\mathrm{N}} \tag{8}$$

In order to use Markov models to predict the transient behaviour of dynamic load. The states of the Markov model are obtained via the clustering algorithm in section 2.1. Here, each cluster of the load along with its set of parameters, $\theta_m = (\mu_m, \sigma_m, w_m)$ represents a single state or "load level" of the Markov model therefore $\underline{\mathrm{N}} = \{C_1, C_2, \ldots C_m, \ldots, C_M\}$.

To build the Markov model the TPM needs to be identified first. Considering Markov property, the probability of observing S_t at the time point t is obtained by (9).

$$\Pr(S_t = s_t) = \Pr(S_1 = s_1) \prod_{t=2}^{T} \Pr(S_t = s_t \mid S_{t-1} = s_{t-1}) \tag{9}$$

Based on the above equation the likelihood of states given a transition probability matrix is defined by (10) where m_{ij} is the number of transitions from state i to state j [39].

$$L(\Lambda, S) = \Pr(S_1 = s_1) \prod_{i=1}^{N} \prod_{j=1}^{N} \lambda_{ij}^{m_{ij}} \tag{10}$$

Therefore, the TPs can be found such that the likelihood function is maximized. Taking the logarithm of the likelihood function and considering the restriction of from the total law of probability $\sum_{j=1}^{N} \lambda_{ij} = 1$, gives the cost function (11) which will be maximized with the TPs given by (12).

$$\log(L(\Lambda, S)) = \log \Pr(S_1 = s_1) + \sum_{i,j=1}^{N} m_{ij} \log \lambda_{ij} + \sum_{i=1}^{j} \left(1 - \sum_{j} \lambda_{ij}\right) \tag{11}$$

$$\lambda_{ij} = \frac{m_{ij}}{\sum_{j=1}^{N} m_{ij}} \tag{12}$$

The summary of the load feature extraction procedure is shown in the flowchart of Fig. 2.

2. 3. Prediction of the Future Load

After clustering the data in historical window and obtaining the features of each cluster, the load levels or states are formed, distinguished and then fed into the Markov model to identify the transient behaviour of the load by constructing a TPM. In order to forecast the load, a procedure reverse to the load characterisation procedure is required which means that based on the current load level at time point t, first the load state, S_{t+1} is predicted via the Markov model and then the load value is generated based on the Gaussian PDF parameters of that state obtained via the GMM.

In the Markov model, the probability of the next state, $S_{t+1} = j$, can be computed by the difference equation in (13).

$$\Pr(S_{t+1}) = \Pr(S_t)^T \Lambda \tag{13}$$

After the Markov state is predicted, the future load value x_{t+1} is obtained via a random data generated from the Gaussian distribution function $N(x; \mu_j, \Sigma_j)$. The initial state for (13) is equal to the state of the Markov model at the last step of modelling.

2. 4. Gaussian-Markov Model Parameter Selection

In the framework proposed for battery load prediction, there exist parameters that need to be addressed properly. Those include the initial conditions, the convergence criteria and the length of the required data.

Here, the initial conditions for clustering algorithm are set equally for all clusters based on the mean and standard deviation of the whole data [40]. Furthermore, the iterative clustering terminates when the difference between the two consecutive estimated parameters becomes less than the predefined threshold or the number of iterations reaches a maximum. These thresholds are set to keep a compromise between the complexity and precision and this study those are 10^{-3} and 25000 respectively.

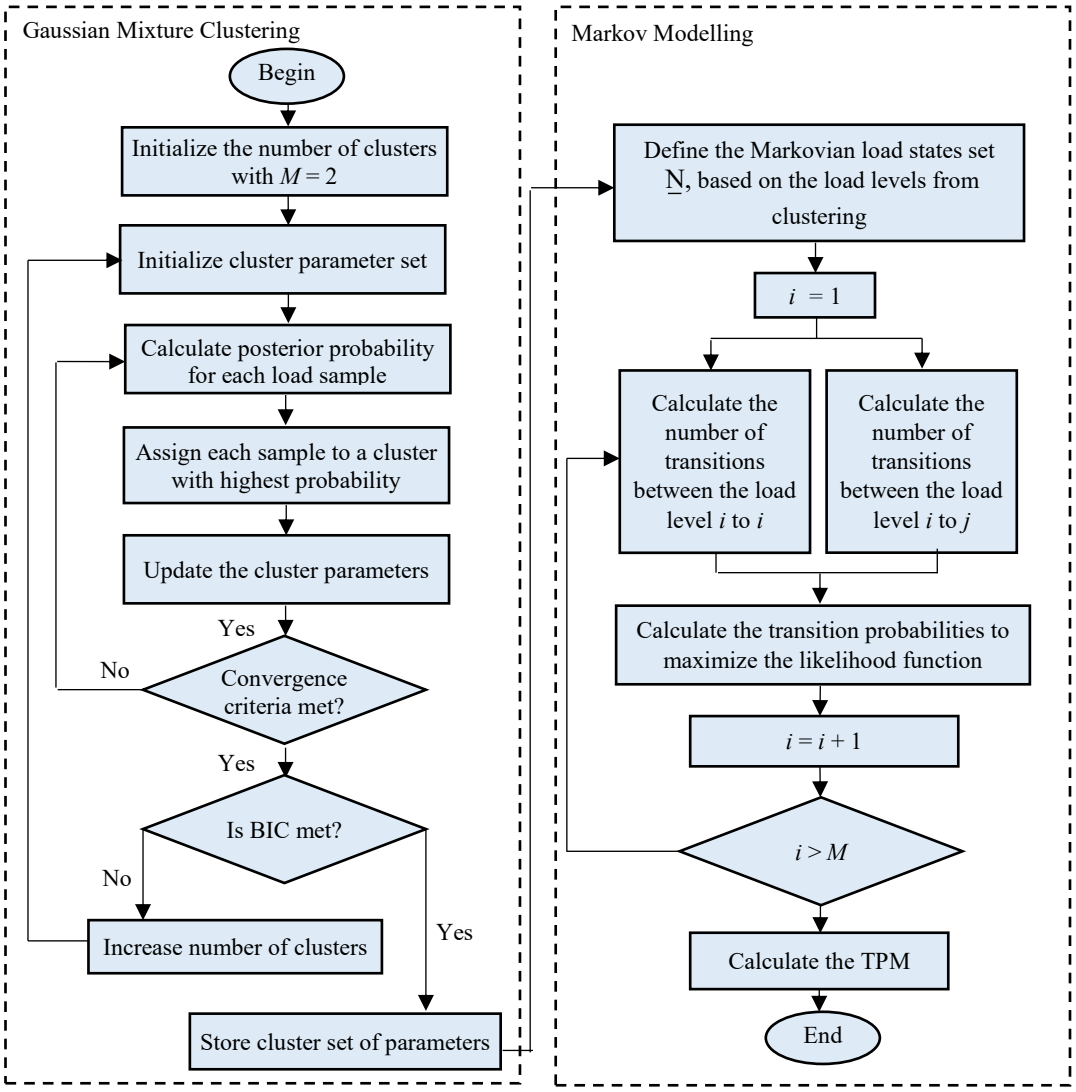

Fig. 2 The load feature extraction mechanism via Gaussian mixture and Markov models

As the EM algorithm may converge to a local minima, multiple runs of clustering algorithm is required to obtained the final set of parameters [41], here the number of runs is set to 5 and the effect of the number of realizations is discussed in the results and discussions section. The number of clusters is also a key variable that affects the computational complexity and the quality of the data clustering. Generally, while large number of clusters may lead to overfitting as well as computational complexity, too few may result in a model unable to represent the whole data properly. Here, the optimum number of clusters is found via Bayesian information criterion (BIC) [42] with the following cost function,

$$J(\theta, M, x) = -2\log L(\theta, x) + \log(T)D(M) \tag{14}$$
$$D(M) = (M-1) + M(d + d(d+1)/2)$$

with d as the dimension of data, $D(M)$ is the number of cluster parameters as a measure for model complexity and the log likelihood function as a measure for quality of fit.

The length of the window including the historical data, *HW*, the update interval, *UI* and the length of the prediction horizon, *PH*, as shown in the Fig. 3 are the other three design variables that need to be addressed properly within the design of the framework.

The length of the prediction window, is automatically determined by the end of discharge criteria of the battery. In other words the prediction is continued until the battery terminal voltage reduces under a predefined threshold. Adjustment of the update interval, *UI*, depends on the application for which the load prediction is performed for.

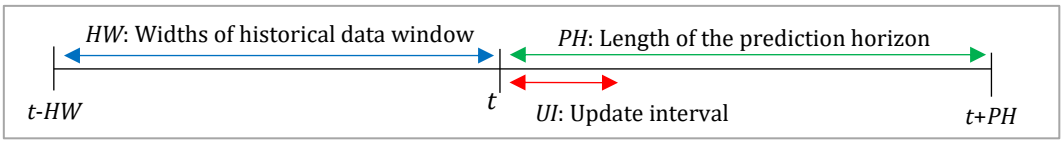

Fig. 3 Load feature extraction and prediction schedule

The remaining energy is a slowly varying signal thus a relatively large update interval can be used. Here initial update interval is set to *UI* = 100 seconds (0.01 Hz) and its effect on the accuracy of the EoDT and RDE prediction is discussed in the results and discussions section. Furthermore, an adaptation mechanism based on the SoC rate, ΔSoC_t of (20) is considered here.

$$\Delta SoC_t = (SoC_t - SoC_{t-HW})\% \tag{15}$$

Generally, the SoC rate depends on the specifications of the load in the historical window, higher rates show that the load demand is high and the battery may reach its end of discharge faster, so in this case the prediction update interval should be small to provide updated information to the BMS more frequently. Smaller SoC rate values imply that the load demand is not very high so a remaining energy estimation with Based on the adaptation mechanism, for $\Delta SoC_t > 5\%$ the update interval of the next prediction step will reduce to $UI/2$.

The width of the data used for training the Gaussian and Markov model, *HW*, also affects the accuracy of prediction. This width is set to a predefined length in the experiments to keep a compromise between the accuracy and complexity. The results for different widths are also given in results and discussions section.

3. Battery Cell Electrical and Thermal Model

RDE calculation requires values for input current, terminal voltage and temperature of the battery both at the present time point and the future. While these signals are easily measurable via a sensor in real – time, their future value can only be accessible through a precise battery model.

The battery is a nonlinear and complex dynamical system with chemical and physical processes. ECMs are proven to be a proper representation of battery, appropriate for use within real-time applications [43]. Due to the computational complexity raised by the long horizon iterative RDE prediction, the model needs to make a compromise between the accuracy and complexity. Therefore, a second order ECM as shown in Fig. 4 is preferred. It includes two branches of resistance R_p, and capacitance C_p that simulate the polarization and diffusion effect of the cell and a serial resistance, R_o to model the internal resistance of the cell and contact resistance of each part.

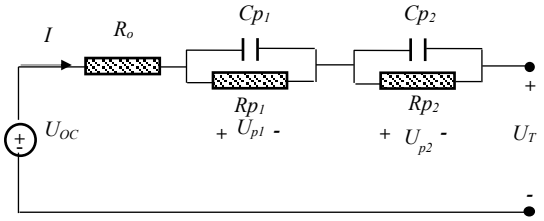

Fig. 4. Second order ECM of the battery cell

U_p is the polarization voltage and OCV is calculated based on empirical data relating OCV to SoC and temperature T (°C). Applying Kirchhoff's law to the electric circuit of the battery and using coulomb counting for SoC estimation, the full set of battery equations can be obtained as (16).

$$\begin{aligned} SoC_t &= SoC_0 - \frac{1}{Q}\int_0^t I_t dt \\ \frac{\partial U_{p_{n,t}}}{\partial t} &= -\frac{U_{p_{n,t}}}{\tau_{n,t}(SoC_t, T_t)} + \frac{I_t}{C_{p_{n,t}}(SoC_t, T_t)} \\ U_{T_t} &= U_{OCt}(SoC_t, T_t) - \sum_{n=1}^{2} U_{p_{n,t}} - R_{o_t}(SoC_t, T_t) I_t \\ \tau_{n,t} &= R_{p_{n,t}}(SoC_t, T_t) C_{p_{n,t}}(SoC_t, T_t) \end{aligned} \tag{16}$$

τ_n is the time constant of each RC branch and n =1, 2 shows the branch index. While the ECM model provides the battery output voltage, a thermal model is used to quantify the local temperature of the cell from t to the EoDT to update the battery set of parameters.

Here, the validated 2-D thermal-impedance model is adopted from [44]. It is assumed that the generated heat is distributed uniformly in the cell and heat conduction and convection are the only forms of heat transfer between the internal cell and the ambient environment. Accordingly, the heat conduction equation is obtained by

$$\rho C_p \frac{\partial T}{\partial t} = q + \frac{1}{r}\frac{\partial}{\partial r}\left(k_r r \frac{\partial T}{\partial r}\right) + \frac{\partial}{\partial z}\left(k_z \frac{\partial T}{\partial z}\right) \tag{17}$$

where ρ is the cell density, C_p is the cell material specific heat capacity, k_r and k_z are the perpendicular and axial thermal conductivity in r and z directions respectively. For a cell with diameter d and length L, r = 0 is the central and $r = d/2$ is the surface location of the cell. Also, z = 0 and $z = L$ are the bottom tab and top tap locations of the cell respectively. q is the volumetric heat generation rate and assumed to be formed of the irreversible heat generation mechanisms only that is heat generation due to reversible mechanisms, enthalpy of mixing, phase change and heat capacity are all negligible. By having the cell measurements, the irreversible heat generation term is obtained as (18) [45], where V_c is the volume of the cell equal to $1/4\pi d^2 L$.

$$q = \frac{I_t(U_{OCt} - U_{T_t})}{V_c} \tag{18}$$

The boundary conditions of for (17) are obtained via the Newton's law of cooling at the cell boundaries as (19) for the top tap, the bottom tap, the external radial surface and the centre of the cell respectively.

$$\begin{aligned} k_z \frac{\partial T}{\partial z}|_{z=L} &= h_{zL}(T_\infty - T_{z=L}) \\ k_z \frac{\partial T}{\partial z}|_{z=0} &= h_{z0}(T_\infty - T_{z=0}) \\ k_r \frac{\partial T}{\partial z}|_{r=d/2} &= h_r(T_\infty - T_{r=d/2}) \\ k_r \frac{\partial T}{\partial z}|_{r=0} &= 0 \end{aligned} \tag{19}$$

While the first three conditions represent the heat transfer at the cell surface, the forth condition is obtained due to the cell symmetry about its core. h_z and h_r are the axial and radial heat transfer coefficients respectively and T_∞ is the temperature of heat transfer fluid. When the cell has both tap and surface cooling, the solution of the heat conduction equation (17) is obtained using the alternating direction implicit method [46, 47], which is widely used within a finite difference simulation approach. The discretised form of equations are described in [44].

Parametrisation of both ECM and thermal model have been done based on experiments and will be fully discussed in the next section. With the battery coupled model, the load prediction and RDE estimation is performed iteratively. The diagram and flowchart of Fig. 5 show the computational mechanism for the EoDT prognosis and the RDE estimation including the load characterization and the reverse mechanism for load prediction.

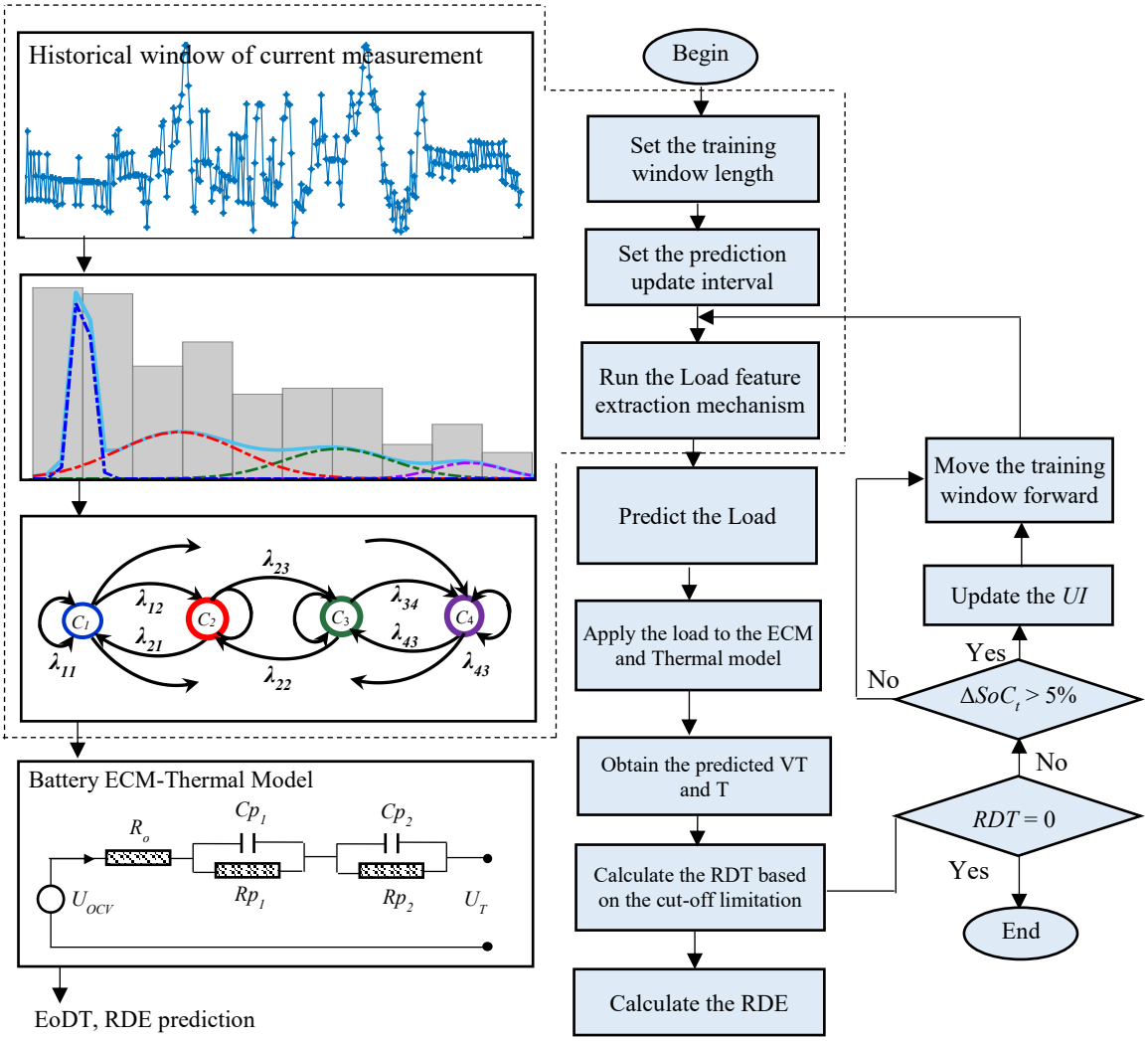

Fig. 5. The flowchart of the whole load prediction, EoDT prognosis and RDE estimation algorithm

4. Experimental Verifications and Discussion

In this study, Lithium-ion cylindrical cells with nickel-manganese-cobalt ($Ni_xMn_yCo_{1-x-y}$) oxide cathode and LiC6 (graphite) anode were used. These cells are widely employed for battery studies as they have relatively smaller capacity in comparison to pouch cells or prismatic cells and therefore required smaller scale equipment and power to reach higher equivalent C-rate. The nominal capacity of the cells is 5.00 Ah, its maximum discharge current is 1.5C (7.275 A) at 25 °C and has a nominal voltage of 3.36 V. Recommended by the manufacturer, the cut-off and maximum allowable voltage are 2.5 and 4.2 V respectively.

Four cells were used for experiments to ensure the consistency of the results and reduce the effect of cell to cell variations. The cells were new and uncycled and had been stored in a thermally managed storage chamber at 10 °C at 50% SoC before experiments to minimize their calendar aging. The cells were horizontally implemented on the test tray and put in the Binder programmable climate chamber to keep the temperature at a desired set-point and limit external temperature fluctuations. On each cell a

thermocouple was placed at the middle height of the outer surface. A Maccor™ series 4000H battery cycler was used to charge and discharge the batteries. A host computer (Intel® Core™ i7-8650U @ 1.90 GHz, 2.11 GHz CPU with 16.0 GB RAM) was used to set the input current profile of the battery, recording the real-time battery signals and the calculations. The test set up is shown in Fig. 6.

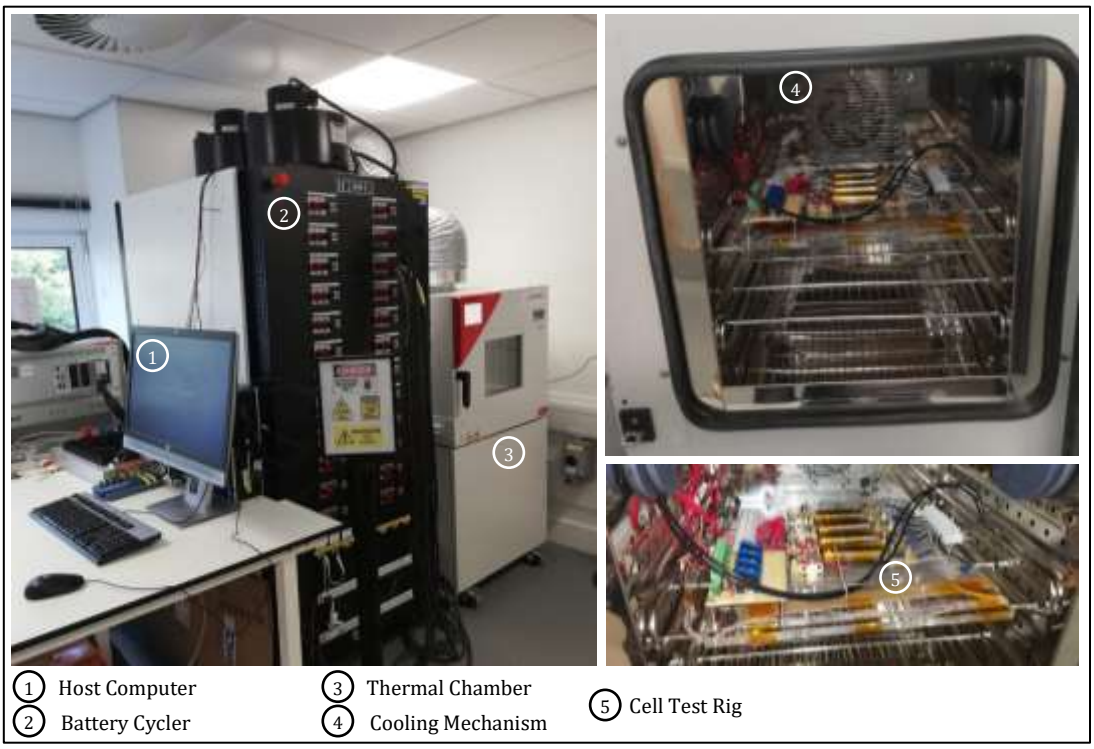

Fig. 6. The experimental battery test set up

4.1. Battery Cell Model Parameterisation and Validation

Before cycling the cells by transient load profiles, cell model parameterisation is performed. The physical specifications of the battery cells are given in Table 1.

Table 1. Physical specification of the battery cell

Cell Parameter	k_z [w m^{-1} K^{-1}]	k_r [w m^{-1} K^{-1}]	C_p [J kg^{-1} K^{-1}]	Cell mass [kg]
Values	30 [48]	0.25 [49]	1050 [50]	0.068
Cell Parameter	d [m]	L [m]	h [w m^{-2} K^{-1}]	Q [Ah]
Values	0.021	0.070	15	5.00

It is noteworthy that battery mass and its dimensions are obtained by experimental measurements. The battery specific heat capacity C_p depends on cell chemistry and selected based on recommendations in [50] which considers the impact of the individual cell layer's properties on the overall specific heat capacity. For the thermal model, according to [51], among all the other parameters of the battery cell, the heat transfer coefficients h_r and h_z, are the most significant parameters that changes the predicted surface temperature and are dependent on the thermal management mechanism applied to the cell. Therefore, while the k_z and k_r values are selected using references [49, 48], $h_r = h_z = h$ value is tuned considering the air forced cooling in the thermal chamber [44].

For cell parameterization, first, the cells are fully discharged with C/5 to the cut off voltage of 2.5, allowed to rest for 4 hours and then fully charged with C/5 via constant current-constant voltage (CC-CV) method. Transition to CV occurred at 2.5 V, with the current terminated when its value reduced to C/100. The current pulse method is used to obtain the cell OCV-SoC curve and the cell model parameters. In this

method a current pulse of C/5 is used to discharge the battery starting from 100% to 0% SoC at each 4% SoC breakpoint. The battery is allowed to equilibrate for 4 hours to ensure that it has reached its steady state before applying the next pulse. The battery response to each pulse provides information about the OCV voltage and the battery dynamics at that SoC. Therefore, via the numerical optimization algorithms [52], the battery model parameters are obtained such that the error between the experimental data and the simulated model is minimized. The cell parameterization is repeated for temperatures 5, 10, 25 and 40 Celsius degrees.

The parameter identification test with 26 discharge and rest cycles is shown in Fig. 7 (for temperature 25 °C as an example). The output of the model with fitted parameters for a second order ECM and its zoomed view are also depicted on this figure. The parameter identification details are on Fig. 7 (c). A sample time of 10ms (0.01 Hz) is employed to minimise errors in the parameterisation process. The fitting quality is illustrated on Fig. 8 with the root mean square (RMS) error of ∓1.85 mV and the maximum error of 221.39 mV; the maximum error is witnessed at the end of the discharge range when the battery is known to become more non-linear. The dependency of the ECM parameters and the OCV to the SoC and temperature are given in Fig. 9; the relationship between the parameters, SoC and temperature shows good stability.

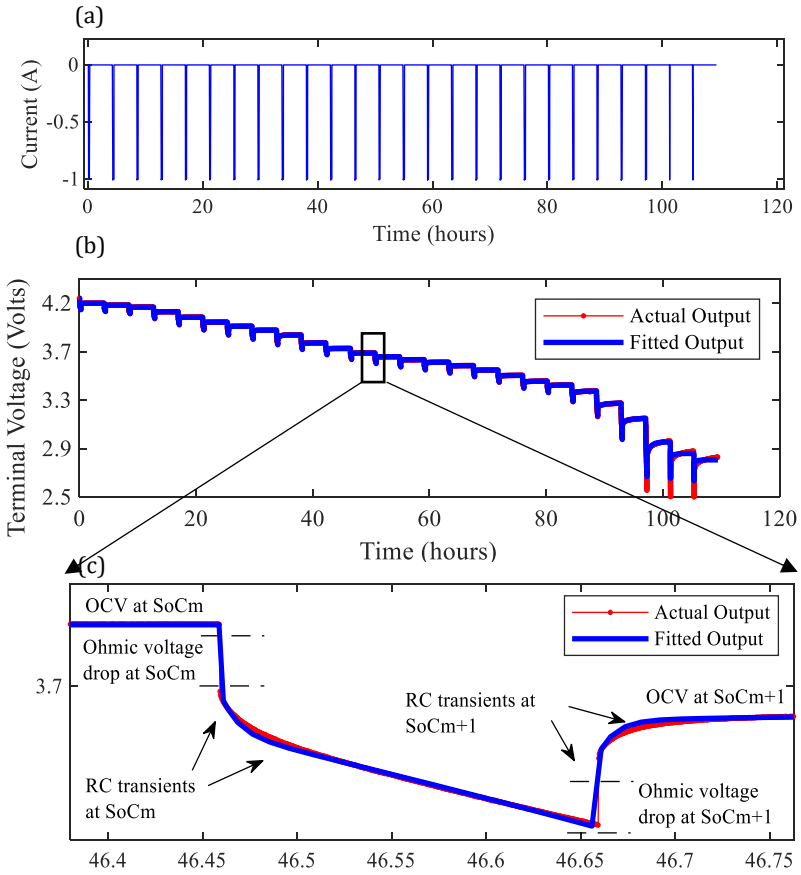

Fig. 7 Battery parameter identification test input (a) the output of the battery and model with fitted parameters (b), the parameter identification details (c) at 25 °C

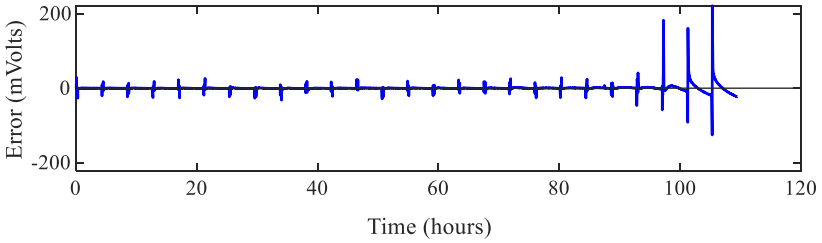

Fig. 8. Battery modelling error at 25 °C

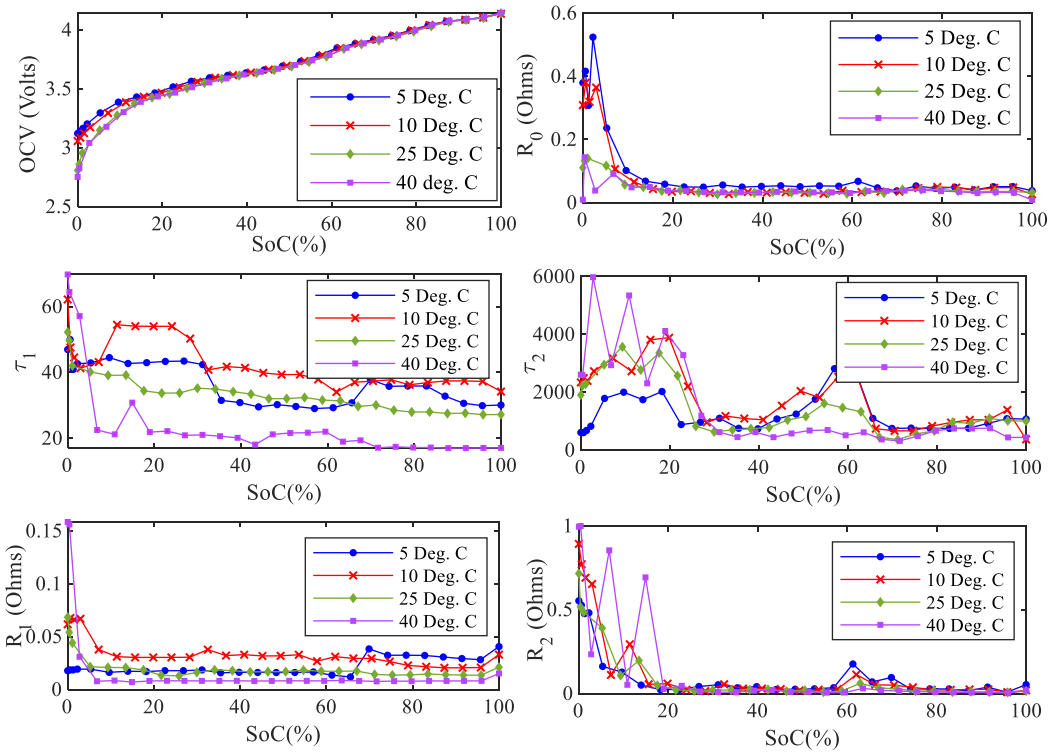

Fig. 9. The parameters of the battery obtained via pulse test for different temperatures

According to the Fig. 9, as the temperature increases the internal resistance of the battery reduces. A similar trend is observed for the relationship between SoC and the resistance, such that the battery internal resistance is increased at lower SoCs. The OCV-SOC relationship with respect to temperature is also compatible with the expectations, in lower temperatures the battery shows reduced capacity to discharge. These parameterisation results are consistent with studies reported in [44, 53].

4.2. EoDT prognosis and RDE estimation under dynamic conditions

In order to validate the performance of the proposed EoDT and RDE prediction method in real-world applications, real drive cycles with transient discharge and some charging events due to the regenerative braking are used here. For this purpose, given the battery pack size, cell requirements and the time-speed profile, a 1-D sizing tool developed by [32] is utilized to quantify the battery input current profile to generate the voltage response. A detailed discussion on the scope and verification of the tool is provided in [32] and will therefore not be repeated here. A typical passenger car (e.g. Nissan Leaf or BMW i3) is taken into account with the maximum battery pack power of 125kw, a minimum energy of 22kwh and a nominal voltage of 350 V.

One benchmark driving cycle (Artemis Motorway), one driving cycle of a real driver in Coventry, United kingdom and a driving cycle which is developed by combining well-known drive cycles (Artemis Motorway, Artemis Urban, High performance EV, real driving cycle) are used. In all validation tests the cells are fully charged with 1C CC-CV method and then discharged via the transient profiles until the recommended cut-off voltage is achieved. The sample time for all cases is set to 1 Hz. Given the nature of the load profiles employed, termination of the experimentation because the cells reaching their thermal limit was not a concern.

As the Gaussian mixture and Markov models are both stochastic models, they provide different results in distinctive realizations. For the results to be more reliable, the number of realizations is selected to be 5 and the average values are reported for EoDT both in minutes and seconds, and for RDE both in Whs and percentage of the maximum extractable energy. The effect of the number of realizations is further discussed at the end of this section.

4.3. Artemis Motorway loading profile at 25°C

In this test the battery was first fully charged to 4.2 V by a 1C current via CC-CV method at 25 °C. The battery was allowed to equilibrate for 2 hours before the discharge test and the chamber temperature was maintained at 25 °C. The Artemis profile was repeated every 1000 seconds to fully discharge the battery. The battery input current, the battery terminal voltage and its temperature are given in Fig. 10. Due to limitations of the battery cycler to generate a load current with a bandwidth greater than circa 1Hz, especially when there is both charge and discharge currents, small variations exist between the desired (simulated) load profile and that actual value applied to the cells under test. Here the actual current applied to the battery via cycler is illustrated and used for the validation.

The actual outputs are compared with the simulated and estimated outputs from the coupled ECM- thermal model. The zoomed view in Fig. 10 shows the accuracy of the model-based estimation results. In this case, the RMS errors of the voltage estimation is 0.03 V and the RMS error of the temperature estimation model is 0.12 °C. The maximum extractable energy at this temperature and load profile is 16.9687 Whs.

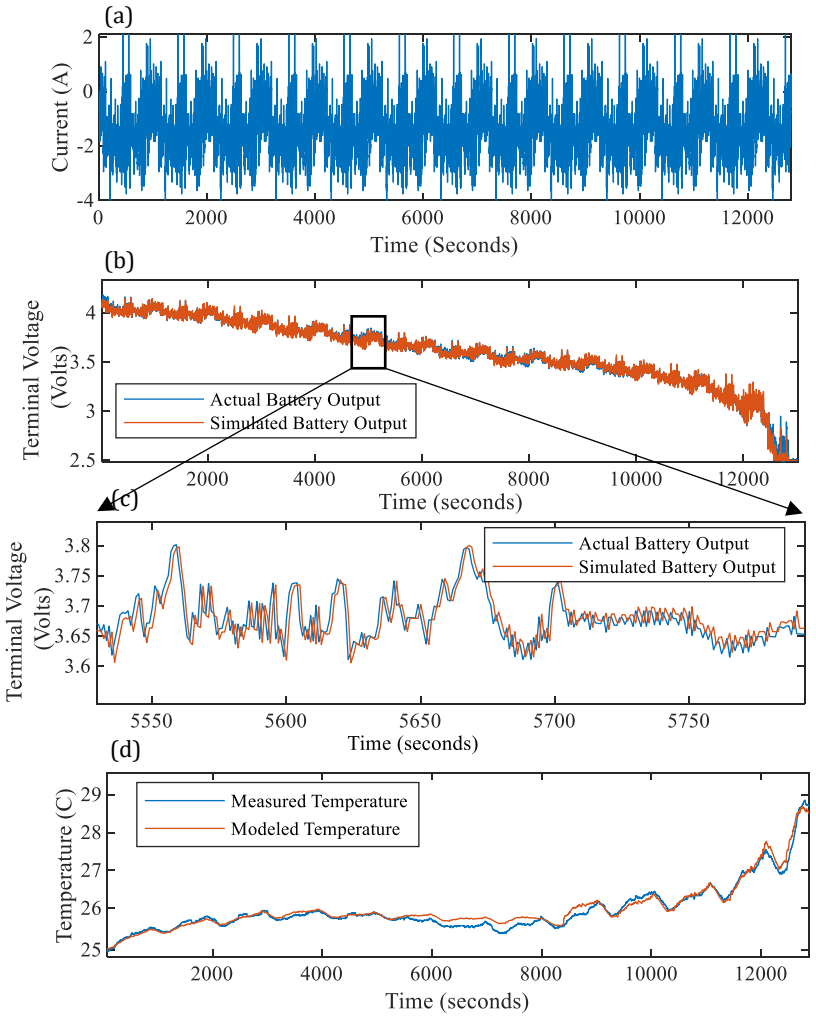

Fig. 10. The battery (a) input current, (b) measured and modeled terminal voltage, (c) zoomed view of measured and modeled terminal voltage, (d) battery measured and modeled temperature under Artemis motorway loading at 25 °C.

Based on the actual input of the battery and the cell ECM-thermal model, load prediction and battery output forecast is performed. To show the merits of the proposed model, the results are compared with those obtained via the mean-based prediction method with the same length of historical data and update rate as a reference case. The length of the historical data for learning is 240 seconds and the update interval is 100

seconds. The number of realizations for the Monte Carlo Gaussian and Markov random generation is set to 5.

A sample prediction of the battery load, terminal voltage, SoC and the battery surface temperature are given in Fig. 11. The extrapolation via the proposed algorithm is depicted by an error bar signal since the algorithm is based on a stochastic model and provides different outputs in distinctive realizations of the model.

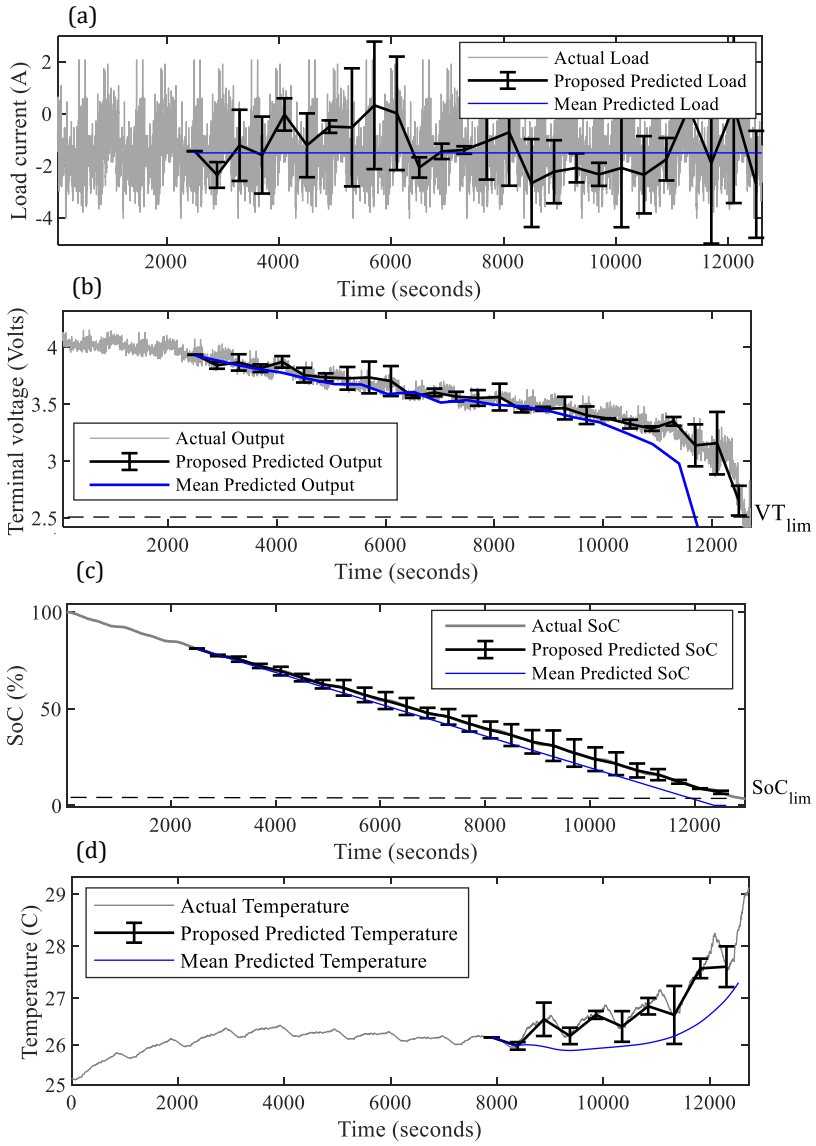

Fig. 11. A sample extrapolation for the proposed and the mean-based method for battery (a) load current, (b) terminal voltage, (c) SoC and (d) temperature under Artemis highway load

The two signals of the proposed and mean-based predicted temperatures have different length as the EoDT for them is obtained differently via the two methods. The end of discharge time prediction results via the designed and mean-based algorithms are given in the Fig. 12.

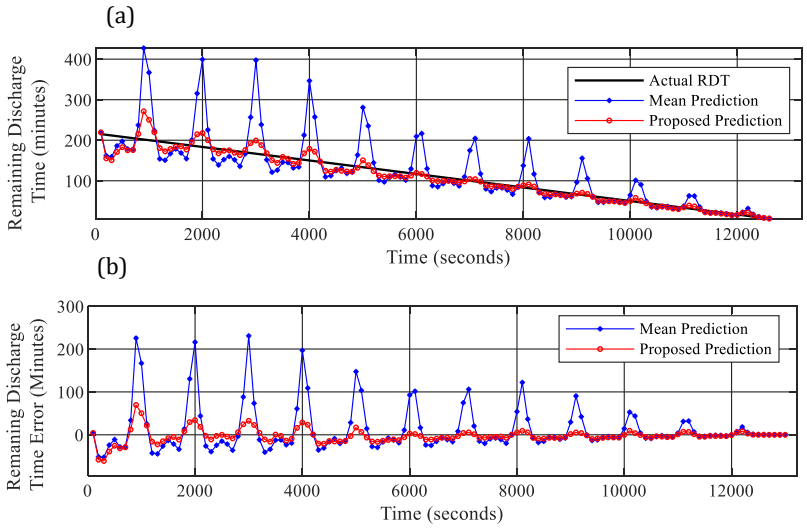

Fig. 12. (a) The RDT prediction results, (b) the remaining discharge time and the end of discharge time prediction errors

The RMS error of the RDT and the end of discharge time prediction is 15.95 minutes (957 seconds) for the proposed prediction while is 55.99 minutes (3359 seconds) for the mean-based method. According to the figure, the mean-based method shows overestimation peaks. Those peaks are smaller for the proposed method. Basically, when mean-based method uses a constant extrapolation for load, proposed method generates multiple scenarios with distinguished load levels and switches between those load levels according to the TPs.

The RDE prediction results are given in Fig. 13, the results are further compared with the DC method. The RMS error for the remaining discharge energy prediction is 5.23 (%) for direct calculation, 1.91 (%) for mean based prediction and 0.36 (%) for proposed prediction.

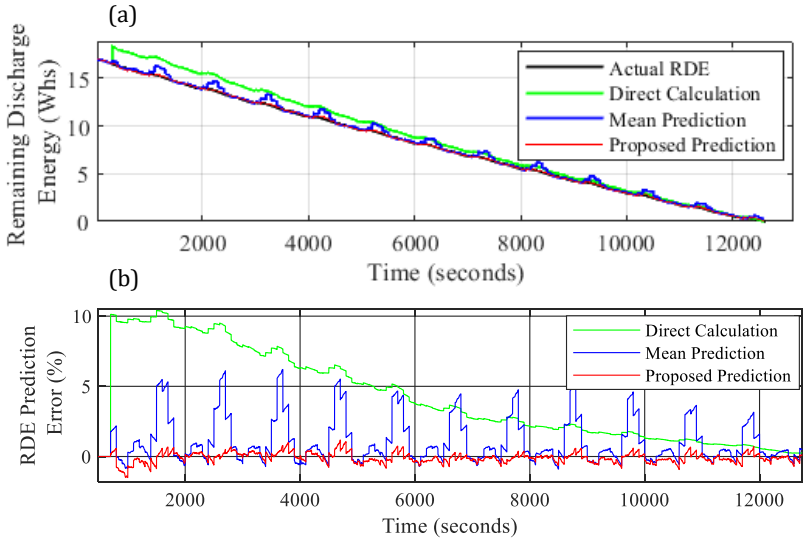

Fig. 13. (a) The RDE prediction results, (b) the remaining discharge energy prediction errors

As the Fig. 13 and 14 show, the error in the predicted RDE is mostly due to the error in the EoDT prognosis. As the proposed method provides a more accurate EoDT prediction, therefore the RDE obtained via this method is closer to the ground truth value. Also it is clear that the error gets smaller as the battery approaches its EoDT, as the signals amplitudes get smaller at this region.

To further investigate the effect of the loading profile specifications on the EoDT and RDE prediction error, a quantitative measure is defined as (20), called the relative transition measure.

$$TL(t_*) = \left| \frac{\mu_2(t_*) - \mu_1(t_*)}{\mu_1(t_*)} \right| \tag{20}$$

Where $\mu_i(t_*)$, $i = 1,2$ are the minimum and maximum cluster centres obtained via clustering method in the range of $t_* \in [t - HW : t]$. $TL(t_*)$ is a unitless quantity considered as transition severity measure. It quantifies how transient the load in the training window is. The absolute error bars of RDT prediction and EoDT prognosis as well as the $TL(t_*)$ values are given in the following figures of Fig. 14. The figure shows that the overestimation peaks of the mean-based prediction method happen exactly in the intervals that the load transition is very high. This is compatible with the incapability of mean-based method to deal with highly transient load profiles. In this case, where relative transition is higher than 10.12 the mean based method cannot provide accurate results.

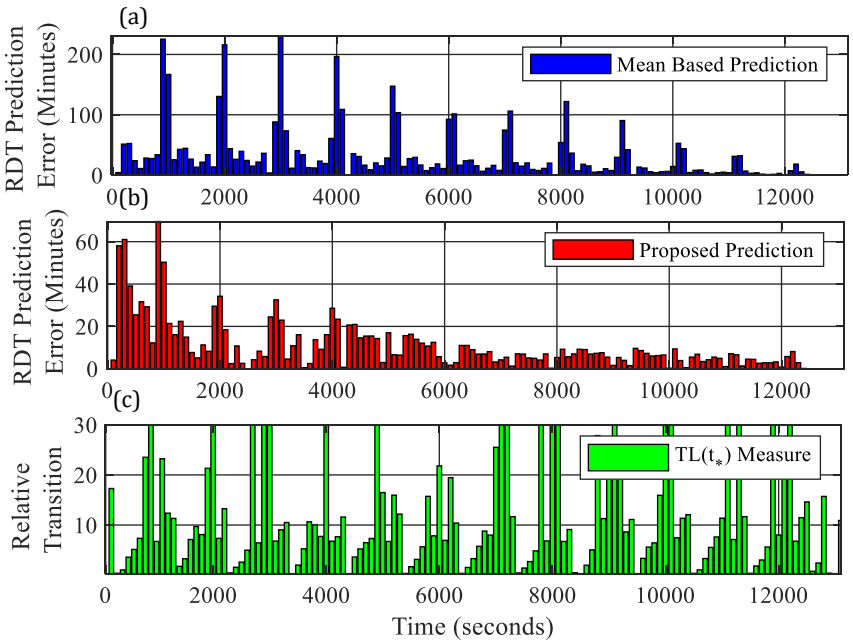

Fig. 14. The EoDT/RDT prediction error bars for (a) mean-based and (b) proposed method, and (c) the relative transition bars for Artemis motorway load profile at 25 °C.

4.4. Coventry motorway loading profile of a real driver at 10°C

For the second load profile, the speed-time data are recorded from a vehicle in the UK city of Coventry and applied to the battery at 10 °C. The length of the original profile was 2642 seconds so it is repeated to achieve enough length of input to take the battery from fully charged to the cut-off limit. The battery input current is depicted in Fig. 15 (a). The measured terminal voltage and temperature of the battery are depicted along with those obtained via the ECM-thermal model are given at Fig. 15 (b-d). The RMS error for the model-based terminal voltage estimation is 0.04 V and for model-based temperature estimation is 0.46 °C. At this temperature and loading conditions, the maximum extractable energy is 16.17 Whs.

A sample extrapolation by the prediction algorithm and the battery model is given at Fig. 16. The capability of the proposed model for extrapolation is compared to that of the mean-based algorithm. As the results show, in some intervals the mean-based method cannot provide accurate results and the extrapolation diverges as the battery gets closes to its end of discharge time where the battery is more nonlinear. The design variables are similar to the previous loading case.

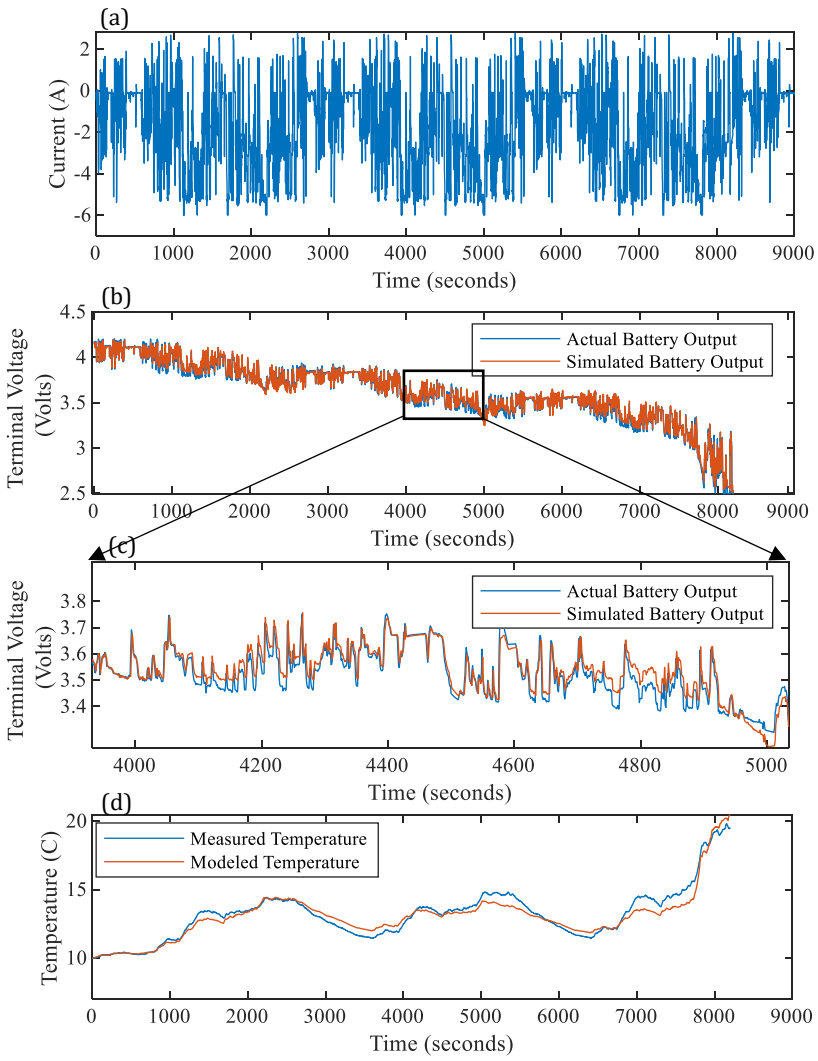

Fig. 15. The battery (a) input current, (b) masured and modeled terminal voltage, (c) zoomed view of measured and modeled terminal voltage, (d) battery measured and modeled temperature under real driver loading profile at 10 °C.

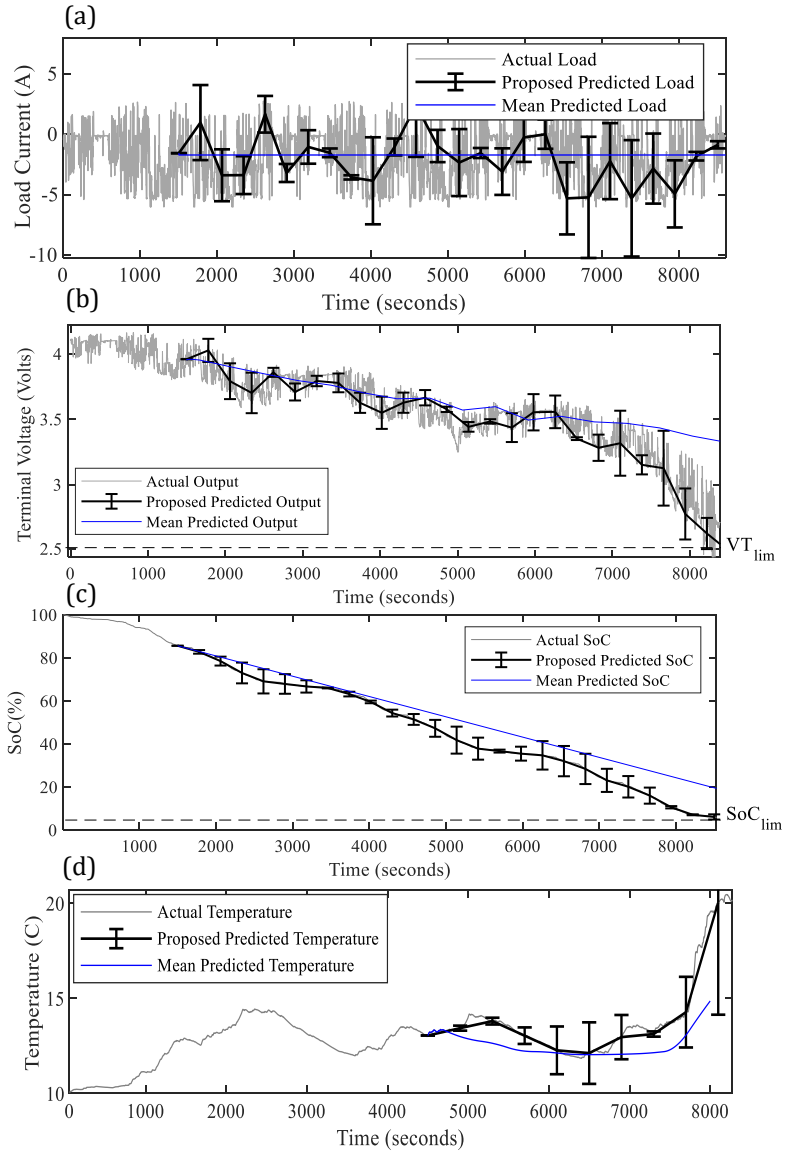

Fig. 16. A sample extrapolation for the proposed and the mean-based method for battery (a) load current, (b) terminal voltage, (c) SoC and (d) temperature under real driver loading profile

The prediction results via the designed and the mean-based algorithms are given in the Fig. 17 and Fig. 18.

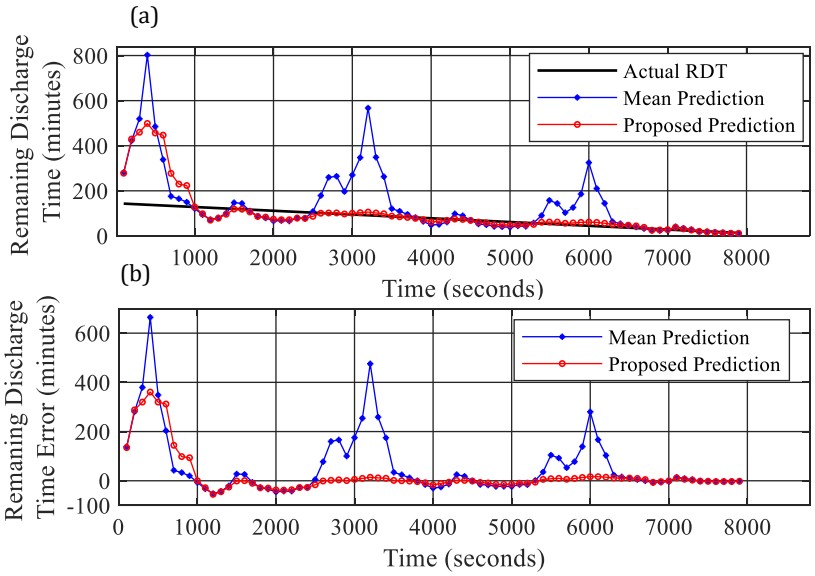

Fig. 17. (a) The remaining discharge time prediction results, (b) the remaining discharge time and the end of discharge time prediction errors for a under real driver loading profile at 10 °C.

In this case, the RMS error of the EoDT and RDT prediction is 86.46 minutes (5187 seconds) for the proposed prediction and 139.10 minutes (8346 seconds) for the mean-based prediction.

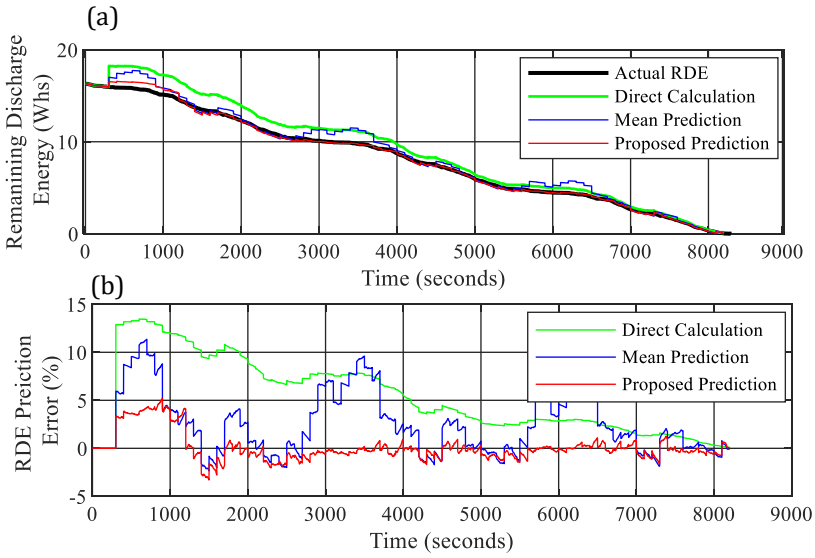

Fig, 18. (a) The remaining discharge energy prediction results, (b) the remaining discharge energy prediction errors for under real driver loading profile at 10 °C

The RMS error for the remaining discharge energy prediction is 6.69 (%) by direct calculation, 4.12 (%) by mean-based method and 1.46 (%) for proposed method. The EoDT/RDT prediction error bars are shown in Fig. 19 accompanied with the values of the relative transitions. As the results show, the error of the mean-based method is higher than the proposed method in high *TL* values. Precisely, in those intervals that the average relative transition measure is higher than 9.81, the proposed method shows a better performance.

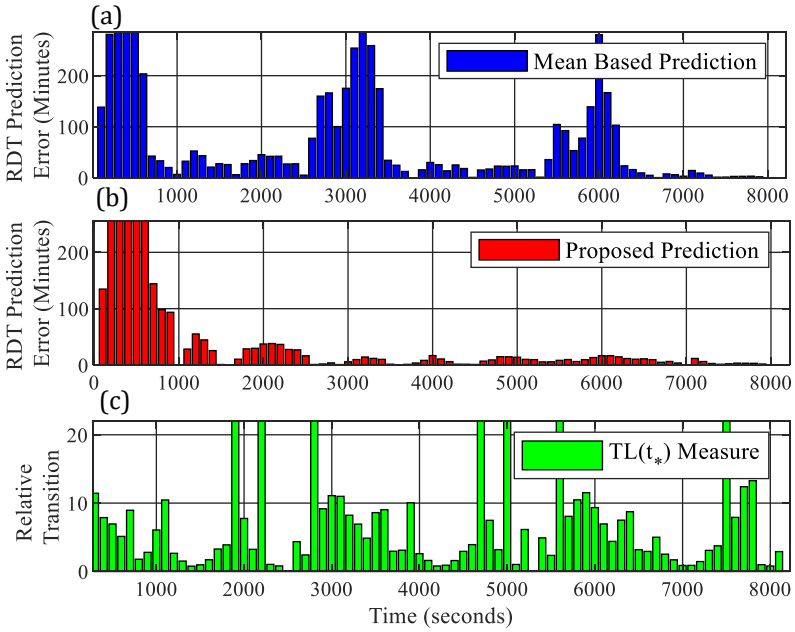

Fig. 19. The EoDT/RDT prediction error bars for (a) Mean based and (b) proposed and (c) the relative transition bars for under real driver loading profile at 10 °C

4.5. Synthetic loading profile at 15°C

To further analyse if the accuracy of the EoDT/RDT and the RDE prediction is affected by the repetitiveness of the load profile, an additional load profile is synthesised and used for prediction. The profile is synthesised by concatenating different charge/discharge current profiles together. This profile is a mixture of currents regarding a high performance (HP) vehicle [54], for 201 seconds, Artemis Urban (AU) for 1033 seconds, Artemis Motorway (AM) for 1000 seconds and the profile from a real driver at Coventry motorway (CM) for 2642 seconds. These sections are stitched together arbitrarily to provide enough length to discharge the battery from fully charges to 2.5 V. The loading profile is illustrated in Fig. 20.

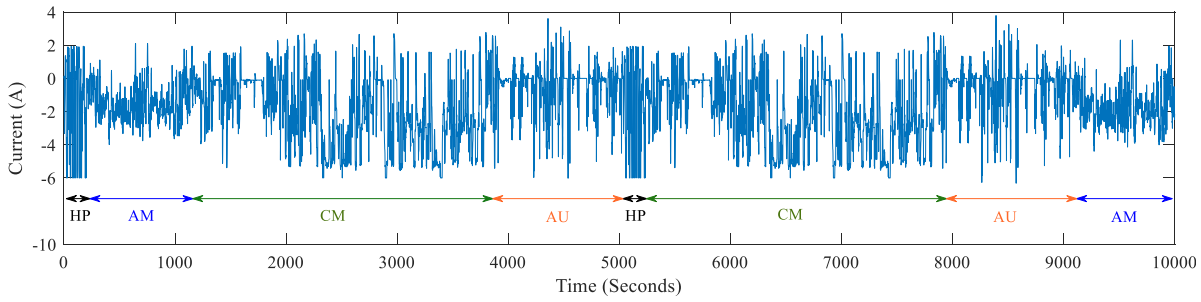

Fig. 20. The non-repetitive synthetic current profile

In Fig. 21, examples of how the clustering algorithm classifies the data of a learning window into a limited number of clusters with Gaussian distribution is given. Evidantly the optimum number of clusters is different for different learning windows. As the results show, the clustering algorithm sucessfully distinguishes the main clusters of the data. The Gaussian distributins in Fig. 21 are all scaled up to be visible when plotted on the data historam. In this case, the length of the learning window is set to 1000 seconds and the number of realizations for the Monte Carlo Gaussian and Markov random generation is set to 5.

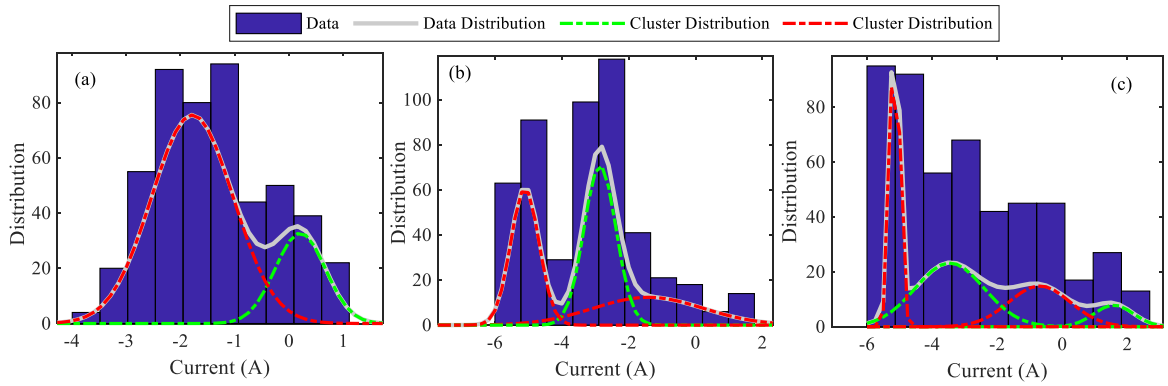

Fig. 21. The data distribution and clusters for intervals of (a) (100, 1100] seconds, (b) (3200, 4200] seconds and (c) (2100, 3100] seconds of the synthetic loading profile

The RDT and RDE prediction results are plotted in the figures of Fig. 22 and Fig. 23 respectively.

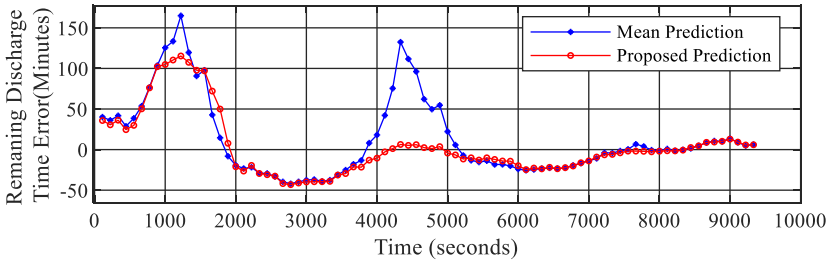

Fig. 22. The remaining discharge time prediction errors for the synthetic loading profile 15 °C.

In this case, the RMS error of the EoDT/RDT prediction is 37.32 minutes (2239 seconds) for the proposed method and 48.82 minutes (2929 seconds) for the mean-based prediction. The RMS error for the remaining discharge energy prediction is 5.91 (%) for DC, 1.66 (%) for mean-based prediction and 0.95 (%) for proposed prediction. The EoDT/RDT prediction error bars are given in Fig. 24; the average relative transition for the better performance of the proposed method is 15.98.

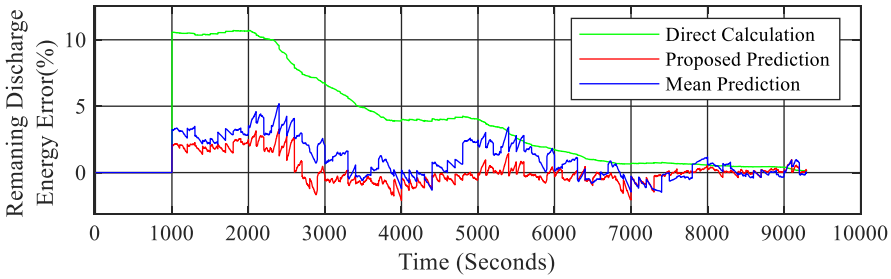

Fig. 23. The remaining discharge energy prediction errors for the synthetic loading profile at 15 °C

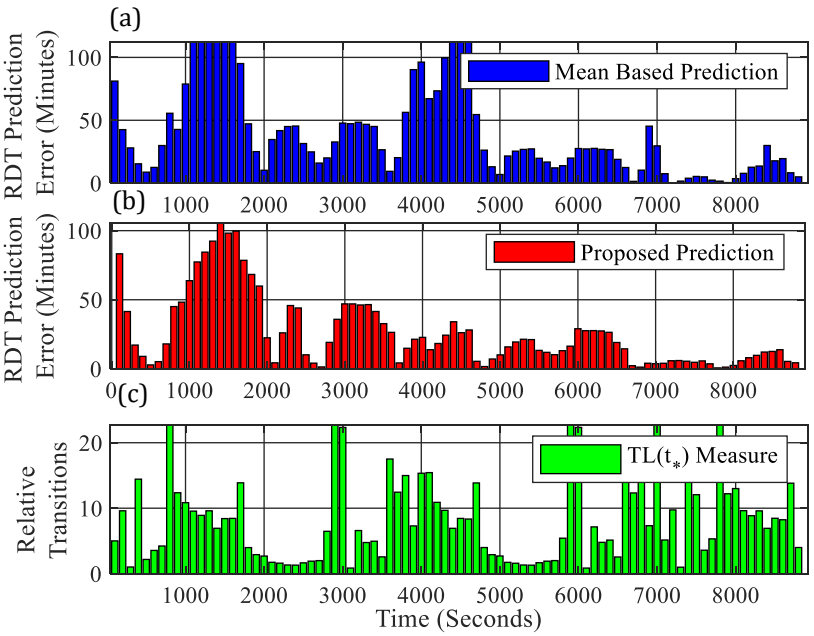

Fig. 24. The EoDT/RDT prediction error bars for (a) Mean based and (b) proposed and (c) the relative transition bars for the synthetic loading profile at 10 °C

For further investigations, the results for the update interval of 50 seconds and historical data of 500 seconds are also given in Fig. 25 and Fig. 26 respectively. The RMS error of the EoDT/RDT prediction is 24.18 minutes (1450 seconds) for the proposed method and 71.83 minutes (4309 seconds) for the mean-based prediction. The RMS error for the RDE prediction is 5.80 (%) for direct calculation, 1.54 (%) for mean-based prediction and 0.93 (%) for proposed prediction. The results show that reducing the update interval can reduce the prediction error at the expense of an increase in the computational load imposed on the real-time processor.

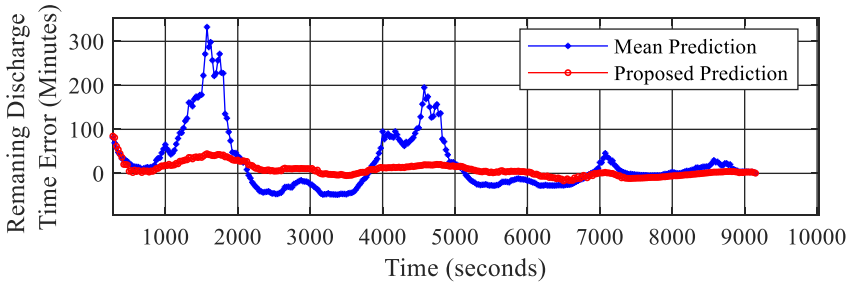

Fig. 25. The EoDT/RDT prediction errors for the synthetic loading profile 15 °C for the learning window length of 500 seconds and update interval of 50 seconds.

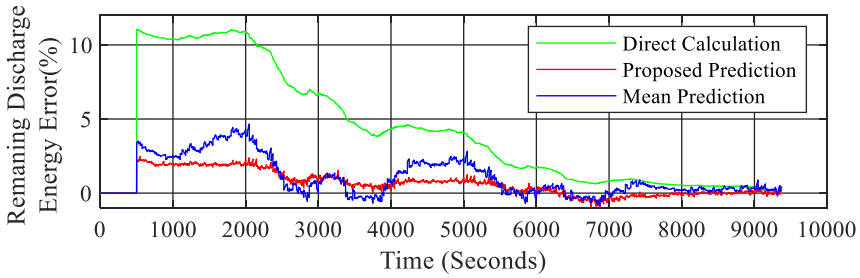

Fig. 26. The RDE prediction errors for the synthetic loading profile 15 °C for the learning window length of 500 seconds and update interval of 50 seconds.

The following tables show how the design variables of the proposed algorithm affect the accuracy of the prediction. For the comparison purposes. For completeness, an estimation of the computation time is also reported.

Table 2 lists the results of calculations with different length of data in historical window and the update interval of 100 seconds. The average computation time over a predefined load profile to fully discharge the battery is 0.2556 seconds. To do a fair comparison, the number of realizations for the Monte Carlo Gaussian and Markov random generation is set to 1. Here, the computation time is the average time required for data clustering, obtaining the Markov model, predicting the load and finally calculating the EoDT and RDE at each update interval.

Table 2. The effect of the historical window length on the accuracy of the predicted values

HW (seconds)	Load Prediction Method	EoDT/RDT RMS error (minutes)	RDE RMS error (%)	Average Computation Time (Seconds)
120	Proposed Prediction	54.903	-1.156	0.807
	Mean Prediction	184.715	-2.018	0.767
240	Proposed Prediction	45.012	-1.153	0.809
	Mean Prediction	108.240	-1.902	0.767
500	Proposed Prediction	36.079	-1.055	0.823
	Mean Prediction	72.844	-1.819	0.813
1000	Proposed Prediction	37.409	-0.9773	0.946
	Mean Prediction	48.828	-1.660	0.876

As the results show, by increasing the length of the data for the learning purposes, the accuracy of the results will increase. However, the computation time will also increases as the size of data grows. This is due to the increased complexity of both Gaussian mixture data clustering and Markov modelling.

The computational complexity of the proposed method for on-board implementation requires special considerations. Both mean-based and proposed algorithms for load prediction are consisted of multiple steps and carried out iteratively. However due to the rather large update intervals, UI, required for the remaining energy and end of discharge time calculations, this computations can be well managed in BMS processors. Obviously more frequent updates can be addressed via cloud computing networks which facilitate remote and off-board calculations and transmit the results to the on-board BMS [55].

Table 3 shows the effect of the update interval length on the accuracy of the results. For obtaining reliable results, the length of the learning window in this case is fixed to 500 seconds and the number of Monte Carlo realizations is set to 1. In this table, the computation time is the total time of prediction for the whole loading profile.

Table 3. The effect of the update interval length on the accuracy of the predicted values

UI (seconds)	Load Prediction Method	EoDT/RDT RMS error (minutes)	RDE RMS error (%)	Total Computation Time (Seconds)
25	Proposed Prediction	17.008	-0.981	264.9181
	Mean Prediction	71.339	-1.657	258.5523
50	Proposed Prediction	24.205	-0.992	132.8544
	Mean Prediction	71.835	-1.697	129.1794
100	Proposed Prediction	36.079	-1.055	68.0036
	Mean Prediction	72.844	-1.819	71.1941
200	Proposed Prediction	47.477	-1.191	33.0359
	Mean Prediction	63.031	-2.067	31.3456

According to the results listed in Table 3, by a more frequent prediction and smaller update intervals, the accuracy of the EoDT and RDE prediction will increase as the Markov forecasts are more accurate at near future. However this has an inverse effect on the total computational time.

The effect of the number of Monte Carlo realizations on the prediction accuracy is analysed in Table 4. For this case the historical data length is 500 and the update range is 100.

Table 4. The effect of the number of Monte Carlo realizations on the accuracy of the predicted values

Monte Carlo Realizations (Number)	EoDT/RDT (minutes)	RDE RMS error (%)	Total Computation Time (Seconds)
1	36.079	-1.055	68.003
3	36.586	-1.082	186.574
5	36.841	-1.102	276.002
7	36.452	-1.062	426.581
10	36.109	-1.075	1540.6

As table 4 shows, by increasing the number of realizations from 1 to 5, the accuracy of the results will increase, however this improvement in both EODT and the RDT is obtained with an increased computation time. For number of realizations more than 5, a negligible improvement in EoDT/RDT error and reduced accuracy in RDE is observed which is believed to be due to the increased uncertainty bound for the results. Based on this analysis the authors determined that the number of realizations equal to 5 provides the best trade-off between speed and performance.

5. Conclusions

The major challenge in battery EoDT/RDT and RDE prediction is the requirement of both present and future states of the system. In this regard, this paper proposes a novel stochastic framework for load prediction and utilizes a coupled ECM-thermal model for forecasting the future values of the battery load current, terminal voltage, its temperature and it's parameter-set. Via this framework ultimately the EoDT based on terminal voltage limitations is obtained and the RDE is estimated. This method removes the fundamental assumption often employed in the literature regarding the *a priori* known load profile for the RDE calculations. It facilitates the forecast of the battery parameters and despite the previous results addresses the SoC and temperature dependency of the parameters for prediction. The method is verified experimentally under different loading conditions and temperatures. The verification results are compared with those of the DC and mean-based prediction methods to show its merits.

6. Future studies

Three primary elements of further work exist for this study. The first is to verify the applicability of the proposed approach within a commercial BMS where the memory is limited by its hardware. For this purpose additional focus on a stack of cells connected in a module or a pack is also required. For a module/pack of batteries there is no need to run the algorithm for each individual cell as the accumulated power of all cells will be delivered to the vehicle ultimately. The main concern for this case would be the uncertainty of battery module/pack model due to the inconsistency between different cells which will negatively affect the EoDT and the remaining energy prediction accuracy. The second area of further work is to repeat this initial study on different battery–types; thereby ensuring the transferability of these results to other cell chemistries and form-factors. The third area is extended experimental verifications via real time vehicle data and traffic information. Today, there exist various technologies such as controller area network (CAN) data logger or global positioning system (GPS) logger for collecting real time data from fleet, upload it to remote cloud server and implement prediction models for analysis purposes. The real time data from vehicles (such as vehicle type, speed, direction, road type, driving lane, and energy consumption) if used along with the historical data and presented stochastic model will help improve the accuracy of the predicted scenarios for future load. Definitely, big data management, as well as cloud/edge computing techniques are prerequisites in this case.

Acknowledgment

The research was undertaken in collaboration with the WMG Centre High Value Manufacturing Catapult (funded by Innovate UK) in collaboration with Jaguar Land Rover Limited.

References

[1] N. Rauh, T. Franke and J. F. Krems, "Understanding the impact of electric vehicle driving experience on range anxiety," *Human factors,* vol. 57, no. 1, pp. 177-187, 2015.

[2] T. Franke, I. Neumann, F. Bühler and P. Cocron, "Experiencing range in an electric vehicle: Understanding psychological barriers," *Applied Psychology,* vol. 61, no. 3, pp. 368-391, 2012.

[3] J. Neubauer and E. Wood, "The impact of range anxiety and home, workplace, and public charging infrastructure on simulated battery electric vehicle lifetime utility," *Journal of power sources,* vol. 257, pp. 12-20, 2014.

[4] M. Hannan, M. Lipu, A. Hussain and A. Mohamed, "A review of lithium-ion battery state of charge estimation and management system in electric vehicle applications: Challenges and recommendations," *Renewable and Sustainable Energy Reviews,* vol. 78, pp. 834-854, 2017.

[5] G. L. Plett, Battery management systems, Volume I: Battery modelling, Artech House, 2015.

[6] C. Campestrini, T. Heil, S. Kosch and A. Jossen, "A comparative study and review of different Kalman filters by applying an enhanced validation method," *Journal of Energy Storage,* vol. 8, pp. 142-159, 2016.

[7] M. Ali, A. Zafar, S. Nengroo, S. Hussain, M. Junaid Alvi and H. Kim, "Towards a smarter battery management system for electric vehicle applications: A critical review of lithium-ion battery state of charge estimation," *Energies,* vol. 12, no. 3, pp. 446-479, 2019.

[8] D. Pola, H. Navarrete, M. Orchard, R. Rabié, M. Cerda, B. Olivares and J. Silva, "Particle-filtering-based discharge time prognosis for lithium-ion batteries with a statistical characterization of use profiles," *IEEE Transactions on Reliability,* vol. 64, no. 2, pp. 710-720, 2015.

[9] C. Sbarufatti, M. Corbetta, M. Giglio and F. Cadin, "Adaptive prognosis of lithium-ion batteries based on the combination of particle filters and radial basis function neural networks," *Journal of Power Sources,* vol. 344, pp. 128-140, 2017.

[10] C. Ley and M. Orchard, "The Impact of Lithium-Ion Battery Polarising Impedance Modelling on End-of-Discharge Prognosis Accuracy," *IFAC-PapersOnLine,* vol. 51, no. 24, pp. 214-220, 2018.

[11] C. Zhang, X. Yu, G. Dong, J. Wei and Z. Chen, "A method for remaining discharge time prediction of lithium-ion batteries under dynamic uncertainty," *International Journal of Energy Research,* vol. 43, no. 5, pp. 1760-1774, 2019.

[12] C. Tampier, A. Pérez, F. Jaramillo, V. Quintero, M. Orchard and J. Silva, "Lithium-ion battery end-of-discharge time estimation and prognosis based on Bayesian algorithms and outer feedback correction loops: A comparative analysis," in *Annual Conference of the PHM Society*, San Diego, CA, USA, 2015.

[13] G. Liu, M. Ouyang, L. Lu, J. Li and J. Hua, "A highly accurate predictive-adaptive method for lithium-ion battery remaining discharge energy prediction in electric vehicle applications," *Applied energy,* vol. 149, pp. 297-314, 2015.

[14] X. Zhang, Y. Wang, C. Liu and Z. Chen, , "A novel approach of remaining discharge energy prediction for large format lithium-ion battery pack," *Journal of Power Sources,* vol. 343, pp. 216-225, 2017.

[15] M. Orchard, G. Kacprzynski, K. Goebel and B. Saha, "Advances in uncertainty representation and management for particle filtering applied to prognostics," in *International Conference on Prognostics and Health Management*, Denver, CO, USA, 2008.

[16] F. Quiñones, R. Milocco and S. Real, "Remaining discharge-time prediction for batteries using the Lambert function," *Journal of Power Sources,* vol. 400, pp. 256-263, 2018.

[17] Z. Chen, H. Sun, G. Dong, J. Wei and J. Wu, "Particle filter-based state-of-charge estimation and remaining-dischargeable-time prediction method for lithium-ion batteries," *Journal of Power Sources,* vol. 414, pp. 158-166, 2019.

[18] R. Xiong, Y. Zhang, H. He, X. Zhou and M. Pecht,, "A double-scale, particle-filtering, energy state prediction algorithm for lithium-ion batteries," *IEEE Transactions on Industrial Electronics,* vol. 65, no. 2, pp. 1526-1538, 2017.

[19] Y. Wang and Z. Chen, "A framework for state-of-charge and remaining discharge time prediction using unscented particle filter," *Applied energy,* vol. 260, p. 114324, 2020.

[20] M. Orchard, "A particle filtering-based framework for on-line fault diagnosis and failure prognosis," Doctoral dissertation, Georgia Institute of Technology, 2007.

[21] M. Orchard, F. Tobar and G. Vachtsevanos, "Outer feedback correction loops in particle filtering-based prognostic algorithms: Statistical performance comparison," *Studies in Informatics and Control,* vol. 18, no. 4, pp. 295-304, 2009.

[22] Y. Wang, D. Yang, X. Zhang and Z. Chen, "Probability based remaining capacity estimation using data-drivenand neural network model," *Journal of Power Sources,* vol. 315, pp. 199-208, 2016.

[23] G. Dong, X. Zhang, C. Zhang and Z. Chen, "A method for state of energy estimation of lithium-ion batteries based on neural network model," *Energy,* vol. 90, no. 1, pp. 879-888, 2015.

[24] X. Liu, J. Wu, C. Zhang and Z. Chen, "A method for state of energy estimation of lithium-ion batteries at dynamic currents and temperatures," *Journal of power sources,* vol. 270, pp. 151-157, 2014.

[25] H. He, Y. Zhang, R. Xiong and C. Wang, "A novel Gaussian model based battery state estimation approach: State-of-Energy," *Applied Energy,* vol. 151, pp. 41-48, 2015.

[26] N. Kim, A. Rousseau and E. Rask, "Parameter estimation for a Lithium-ion battery from chassis dynamometer tests," *IEEE Transactions on Vehicular Technology,* vol. 65, no. 6 , pp. 4393-4400, 2015.

[27] R. Wang and S. Lukic, "Review of driving conditions prediction and driving style recognition based control algorithms for hybrid electric vehicles," in *IEEE Vehicle Power and Propulsion Conference*, Chicago, IL, USA, 2011.

[28] C. Martinez, M. Heucke, F. Wang, B. Gao and D. Cao, "Driving style recognition for intelligent vehicle control and advanced driver assistance: A survey," *IEEE Transactions on Intelligent Transportation Systems,* vol. 19, no. 3, pp. 666-676, 2017.

[29] C. De Cauwer, J. Van Mierlo and T. Coosemans, "Energy consumption prediction for electric vehicles based on real-world data," *Energies,* vol. 8, no. 8, pp. 8573-8593, 2015.

[30] D. Ren, L. Lu, P. Shen, X. Feng, X. Han and M. Ouyang, "Battery remaining discharge energy estimation based on prediction of future operating conditions," *Journal of Energy Storage,* vol. 25, p. 100836, 2019.

[31] G. Dong, J. Wei, Z. Chen, H. Sun and X. Yu, "Remaining dischargeable time prediction for lithium-ion batteries using unscented Kalman filter," *Journal of Power Sources,* vol. 364, pp. 316-327, 2017.

[32] J. Taylor, R. Ball, A. McGordon, K. Uddin and J. Marco, "Sizing tool for rapid optimisation of pack configuration at early-stage automotive product development," *World Electric Vehicle Journal,* vol. 7, no. 1, pp. 93-100, 2015.

[33] S. Yan, J. Liu, H. Huang and X. Tai, "A dual EM algorithm for TV regularized Gaussian mixture model in image segmentation," *Inverse Problems & Imaging,* vol. 13, no. 3, pp. 653-677, 2019.

[34] I. Shahin, A. Nassif and S. Hamsa, "Emotion Recognition Using Hybrid Gaussian Mixture Model and Deep Neural Network," *IEEE Access,* vol. 7, pp. 26777-26787, 2019.

[35] L. Li, J. Sun, C. Wang, Y. Zhou and K. Lin, "Enhanced Gaussian process mixture model for short-term electric load forecasting," *Information Sciences,* vol. 477, pp. 386-398, 2019.

[36] C. Bishop, Pattern recognition and machine learning, Springer Science+ Business Media, 2006.

[37] A. Dempster, "Maximum likelihood estimation from incomplete data via the EM algorithm," *Journal of the Royal Statistical Society: Series B (Statistical Methodology),* vol. 39, pp. 1-38, 1977.

[38] D. Stroock, An introduction to Markov processes, Springer Science & Business Media, 2013.

[39] Y. Cao, X. Wei, H. Dai and Q. Fang, "A Method for Remaining Discharge Energy Prediction of Lithium-Ion Batteries Based on Terminal Voltage Prediction Model," in *IEEE Vehicle Power and Propulsion Conference*, Belfort, France , 2017.

[40] E. Shireman, D. Steinley and M. Brusco, "Examining the effect of initialization strategies on the performance of Gaussian mixture modeling," *Behavior research methods,* vol. 49, no. 1, pp. 282-293, 2017.

[41] J. Friedman, T. Hastie and R. Tibshirani, The Elements of Statistical Learning, Springer series in statistics, 2001.

[42] G. Schwarz, "Estimating the dimension of a model," *The annals of statistics,* vol. 6, no. 2, pp. 461-464, 1978.

[43] H. He, R. Xiong and J. Fan, "Evaluation of lithium-ion battery equivalent circuit models for state of charge estimation by an experimental approach," *energies,* vol. 4, no. 4, pp. 582-598, 2011.

[44] D. Worwood, Q. Kellner, M. Wojtala, W. Widanage, R. McGlen, D. Greenwood and J. Marco, "A new approach to the internal thermal management of cylindrical battery cells for automotive applications," *Journal of Power Sources,* vol. 346, pp. 151-166, 2017.

[45] K. Onda, T. Ohshima, M. Nakayama, K. Fukuda and T. Araki, "Thermal behavior of small lithium-ion battery during rapid charge and discharge cycles," *Journal of Power sources,* vol. 158, no. 1, pp. 535-542, 2006.

[46] R. Schneider, "Explicit and implicit finite-difference methods for the diffusion equation in two dimensions," Forschungszentrum Karlsruhe GmbH Technik und Umwelt (Germany). Inst. fuer Hochleistungsimpuls-und Mikrowellentechnik., 2003.

[47] L. Song and J. Evans, "Electrochemical-thermal model of lithium polymer batteries," *Journal of the Electrochemical Society,* vol. 147, no. 6, pp. 2086-2095, 2000.

[48] S. Drake, D. Wetz, J. Ostanek, S. Miller, J. Heinzel and A. Jain, "Measurement of anisotropic thermophysical properties of cylindrical Li-ion cells," *Journal of Power Sources,* vol. 252, pp. 298-304, 2014 .

[49] K. Shah, C. McKee, D. Chalise and A. Jain, "Experimental and numerical investigation of core cooling of Li-ion cells using heat pipes," *Energy,* vol. 113, pp. 852-860, 2016.

[50] A. Loges, S. Herberger, P. Seegert and T. Wetzel, "A study on specific heat capacities of Li-ion cell components and their influence on thermal management," *Journal of Power Sources,* vol. 336, pp. 341-350, 2016.

[51] Y. Kim, J. Siegel and A. Stefanopoulou, "A computationally efficient thermal model of cylindrical battery cells for the estimation of radially distributed temperatures," in *American Control Conference*, Washington, DC, USA, 2013.

[52] R. Jackey, M. Saginaw, P. Sanghvi, J. Gazzarri, T. Huria and M. Ceraolo, "Battery model parameter estimation using a layered technique: an example using a lithium iron phosphate cell," *SAE Technical Paper,* Vols. 2013-01-1547, p. 1547, 2013.

[53] V. Sangwan, A. Sharma, R. Kumar and A. Rathore, "Model-based optimal parameter identification incorporating C-rate, state of charge and temperature effect for advance battery management system in electric vehicles," *IET Electrical Systems in Transportation,* vol. 8, no. 4, pp. 240-250, 2018.

[54] Q. Kellner, E. Hosseinzadeh, G. Chouchelamane , W. Widanage and J. Marco, "Battery cycle life test development for high-performance electric vehicle applications," *Journal of Energy Storage,* vol. 15, pp. 228-244, 2018.

[55] H. Khayyam, J. Abawajy, B. Javadi and A. Goscinski, "Intelligent battery energy management and control for vehicle-to-grid via cloud computing network," *Applied energy,* vol. 111, pp. 971-981, 2013.